


# Zn-induced layer exchange of p- and n-type nanocrystalline SiGe layers for flexible thermoelectrics

Cite as: Appl. Phys. Lett. **116**, 182105 (2020); <https://doi.org/10.1063/5.0006958>

Submitted: 07 March 2020 • Accepted: 17 April 2020 • Published Online: 04 May 2020

M. Tsuji, K. Kusano,  T. Suemasu, et al.

## COLLECTIONS

 This paper was selected as Featured



View Online



Export Citation



CrossMark

## ARTICLES YOU MAY BE INTERESTED IN

[Role of tungsten dopants in indium oxide thin-film transistor on radiation hardness technology](#)

Applied Physics Letters **116**, 182104 (2020); <https://doi.org/10.1063/1.5142557>

[Electron spin resonance spectroscopy with femtoliter detection volume](#)

Applied Physics Letters **116**, 184002 (2020); <https://doi.org/10.1063/5.0004322>

[Influence of grain boundaries on the properties of polycrystalline germanium](#)

Journal of Applied Physics **128**, 075301 (2020); <https://doi.org/10.1063/5.0006469>



Webinar  
Quantum Material Characterization  
for Streamlined Qubit Development



[Register now](#)

# Zn-induced layer exchange of p- and n-type nanocrystalline SiGe layers for flexible thermoelectrics

Cite as: Appl. Phys. Lett. **116**, 182105 (2020); doi: [10.1063/5.0006958](https://doi.org/10.1063/5.0006958)

Submitted: 7 March 2020 · Accepted: 17 April 2020 ·

Published Online: 4 May 2020



View Online



Export Citation



CrossMark

M. Tsuji,<sup>1</sup> K. Kusano,<sup>1</sup> T. Suemasu,<sup>1</sup>  and K. Toko<sup>1,2,a)</sup> 

## AFFILIATIONS

<sup>1</sup>Institute of Applied Physics, University of Tsukuba, 1-1-1 Tennodai, Tsukuba, Ibaraki 305-8573, Japan

<sup>2</sup>PRESTO, Japan Science and Technology Agency, 4-1-8 Honcho, Kawaguchi, Saitama 332-0012, Japan

<sup>a)</sup> Author to whom correspondence should be addressed: [toko@bk.tsukuba.ac.jp](mailto:toko@bk.tsukuba.ac.jp)

## ABSTRACT

Fermi-level control in a polycrystalline SiGe layer is challenging, especially under a low thermal budget owing to the low activation rate of impurities and defect-induced acceptors. Here, we demonstrate the low-temperature (120–350 °C) synthesis of nanocrystalline p- and n-type  $\text{Si}_{1-x}\text{Ge}_x$  ( $x: 0-1$ ) layers using the layer exchange technique with a Zn catalyst. Pure Zn formed p-type SiGe layers (hole concentration:  $10^{20} \text{ cm}^{-3}$  for  $x \geq 0.8$ ) due to the shallow acceptor level of Zn in Ge. Conversely, As-doped Zn allowed us to synthesize n-type SiGe layers (electron concentration:  $10^{19} \text{ cm}^{-3}$  for  $x \leq 0.3$ ) at the lowest ever temperature of 350 °C, owing to the self-organized As doping to SiGe during layer exchange. The resulting p-type  $\text{Si}_{0.2}\text{Ge}_{0.8}$  and n-type  $\text{Si}_{0.85}\text{Ge}_{0.15}$  layers exhibited the largest ever power factors ( $280 \mu\text{W/mK}^2$  for the p-type and  $15 \mu\text{W/mK}^2$  for the n-type), for SiGe fabricated on a flexible plastic sheet. The low-temperature synthesis technology, for both p- and n-type SiGe layers, opens up the possibility of developing human-friendly, highly reliable, flexible devices including thermoelectric sheets.

Published under license by AIP Publishing. <https://doi.org/10.1063/5.0006958>

Flexible thermoelectric generators (TEGs) are a key energy harvesting technology for ubiquitous sensors and wearable devices for the future internet of things (IoT) society.<sup>1</sup> Group IV semiconductors, including Si and Ge, are materials suitable for electronic devices close to humans because they are non-toxic and relatively abundant. SiGe alloy is the most reliable thermoelectric material, which has been used for decades due to its large Seebeck coefficient  $S$  and low thermal conductivity  $\kappa$ .<sup>2,3</sup> Thin-film thermoelectric applications of SiGe have been studied using sputtering,<sup>4,5</sup> chemical vapor deposition,<sup>6–8</sup> electrophoretic deposition,<sup>9</sup> solid-phase crystallization,<sup>10</sup> and metal-induced crystallization.<sup>11</sup> Both p- and n-type SiGe layers must be formed at temperatures below the heat-resistant temperature of plastic substrates (e.g., 400 °C for polyimide) to develop SiGe into flexible TEGs. However, SiGe generally requires high temperatures for crystallization and dopant activation, which are essential for improving its thermoelectric properties.<sup>2,3</sup> N-type SiGe layers are formed at especially high temperatures ( $\geq 1000$  °C)<sup>4,8,9</sup> because of the low activation rate of n-type dopants<sup>12</sup> and defect-induced acceptors due to the incorporation of Ge.<sup>13,14</sup> Hence, synthesizing high-thermoelectric performance SiGe at low fabrication temperatures is quite challenging.

Metal-induced layer exchange (LE) is a promising technique for overcoming this problem. The LE technique can crystallize amorphous group IV materials, including Si,<sup>15–18</sup> Ge,<sup>19–24</sup> and C,<sup>25,26</sup> on arbitrary substrates at low temperatures. LE using an Al catalyst is effective also for SiGe alloy.<sup>27–32</sup> We have synthesized SiGe layers at  $\leq 400$  °C in the whole composition range using Al-induced LE and found that Al is highly doped and activated in SiGe according to the solid solubility limit.<sup>33</sup> The resulting p-type SiGe layer formed on a plastic substrate exhibited a power factor ( $PF$ ) of  $190 \mu\text{W/mK}^2$ ,<sup>34</sup> which was improved to  $240 \mu\text{W/mK}^2$  by self-organized B doping during LE.<sup>35</sup> Thus, Al is suitable for p-type SiGe layers with high thermoelectric performance, but is unsuitable for n-type layers because Al acts as an acceptor for SiGe.

In a recent study, we discovered an ultralow-temperature (80 °C) LE in the Ge–Zn system.<sup>36</sup> The resulting Ge on a plastic substrate was highly p-doped because Zn provided shallow acceptor levels for Ge.<sup>37</sup> and exhibited a  $PF$  of  $160 \mu\text{W/mK}^2$ . The  $PF$  value is the highest in thermoelectric films synthesized over such a low-temperature range. However, considering  $\kappa$ , SiGe inducing alloy phonon scattering is preferred over pure Ge. Further, since Zn does not act as a dopant for

Si,<sup>37</sup> n-type conduction control may be possible in Si-rich SiGe by doping impurities. It is owing to the above reasons that this study investigates (i) the application of Zn-induced LE to the entire composition range of SiGe and (ii) controlling n-type conduction by As doping during LE. We demonstrate the synthesis of the n-type SiGe layer at the lowest temperature ever achieved and record the *PF* values for both p and n-type SiGe layers formed on a plastic substrate.

The schematic diagram for this study is shown in Fig. 1. The Zn and amorphous (a-)  $\text{Si}_{1-x}\text{Ge}_x$  ( $x$ : 0, 0.15, 0.3, 0.6, 0.8, and 1) layers (50 nm thick each) were sequentially prepared on a  $\text{SiO}_2$  glass substrate at room temperature (RT) using radio frequency (RF) magnetron sputtering (base pressure  $3.0 \times 10^{-4}$  Pa) with an Ar plasma. The RF power was set to 50 W. The samples were then annealed at 350 °C (15 h) for  $x=0-0.3$ , 300 °C (10 h) for  $x=0.6$  and 0.8, and 120 °C (30 h) for  $x=1$  in an  $\text{N}_2$  ambient furnace. The Zn layer was then etched away using a HCl solution (HCl: 36%) for 20 s. Using the same procedure, for  $x=0-0.3$ , As-doped Zn (As concentration:  $\sim 10\%$ ) was prepared (instead of Zn), to form n-type SiGe layers. The crystal quality of the resulting SiGe was characterized by Nomarski optical microscopy, Raman spectroscopy (wavelength: 532 nm), and electron backscattering diffraction (EBSD) analyses. The electrical properties were characterized by Hall effect measurements using the Van der Pauw method. Thermoelectric measurements were performed using an Advance-Riko ZEM system, where the sample was fixed to a ceramic stage using Ag paste.<sup>34</sup>

The LE was determined by *in situ* optical microscopy observation and the naked eye. Although the required growth temperature increased with decreasing  $x$  according to the basic properties of  $\text{Si}_{1-x}\text{Ge}_x$ ,<sup>14,33</sup> the LE was completed at low temperatures ( $\leq 350$  °C) for all samples. After the removal of Zn, the layers remaining on the substrates were evaluated via Nomarski optical microscopy and Raman spectroscopy. Figure 2(a) shows that the growth morphology is slightly different depending on  $x$ ; some cover almost the entire substrate, while others have noticeable holes. Figure 2(b) shows Raman peaks corresponding to Si-Si, Si-Ge, and Ge-Ge vibration modes, which indicate that crystalline  $\text{Si}_{1-x}\text{Ge}_x$  layers are formed on the substrates by LE for all samples. The SiGe compositions, calculated from the Raman spectra using the equation proposed by Mooney *et al.*,<sup>38</sup> were consistent with those of the as-prepared a- $\text{Si}_{1-x}\text{Ge}_x$  layers determined by Rutherford backscattering spectrometry. Thus, Zn-induced LE was effective for low-temperature crystallization in the entire SiGe composition range.

The grain size of the  $\text{Si}_{1-x}\text{Ge}_x$  layers was evaluated using EBSD analyses. The inverse pole figure (IPF) images in Fig. 3 show the random orientation of the SiGe layers in the whole composition. The samples with the intermediate compositions ( $x=0.3$  and 0.6) exhibit grains that are a few hundred nm in size, while the other samples

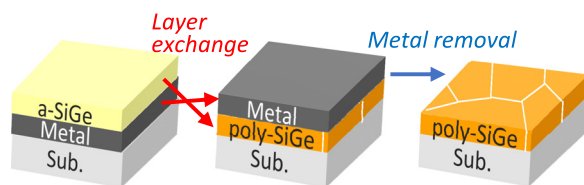


**FIG. 1.** Schematic diagram of the sample preparation procedure. The metal layer could be either Zn or As-doped Zn, while the substrate is either glass or plastic.

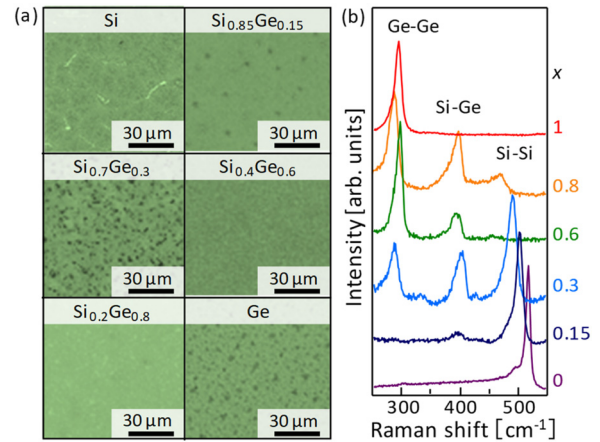


**FIG. 2.** Characterization of  $\text{Si}_{1-x}\text{Ge}_x$  ( $x$ : 0, 0.15, 0.3, 0.6, 0.8, and 1) formed by LE using pure Zn on glass, where Zn layers were removed. (a) Nomarski optical micrographs. (b) Raman spectra.

( $x=0, 0.15, 0.8$ , and 1) exhibit grains that smaller than the EBSD detection limit in the most of the regions. The grains are smaller than those of  $\text{Si}_{1-x}\text{Ge}_x$  formed by other LE using Al,<sup>20,32</sup> Ag,<sup>23</sup> and Au.<sup>21,24</sup> This behavior indicates the high nucleation rate of  $\text{Si}_{1-x}\text{Ge}_x$  in Zn, which causes low temperature crystallization. This is an advantage of Zn-induced LE as TEGs because nanocrystalline grains scatter phonons and significantly lower  $\kappa$ .<sup>7,8,39</sup> In fact, the cross-plane  $\kappa$  of Ge formed by Zn-induced LE was  $2.95 \text{ W mK}^{-1}$ , which is an order of magnitude smaller than  $\kappa$  for bulk-Ge.<sup>2</sup> In the SiGe alloys, lower  $\kappa$  is expected owing to the effect of alloy phonon scattering.<sup>2</sup>

The Hall effect measurement revealed that  $\text{Si}_{1-x}\text{Ge}_x$  formed by LE with pure Zn exhibited p-type conduction in the whole composition except Si whose resistivity was too high to measure. Figure 4(a) shows that hole concentration  $p$  increases with increasing  $x$ . This behavior is probably due to the fact that Zn forms shallow acceptor levels in Ge, but not in Si, as shown in the band diagrams in Fig. 4(a).<sup>37</sup> The electrical conductivity  $\sigma$  also increases with increasing  $x$  because  $\sigma$  is proportional to  $p$ . We evaluated the measurement temperature  $T$  dependence of  $\sigma$  and found that  $\sigma$  exhibited a more positive

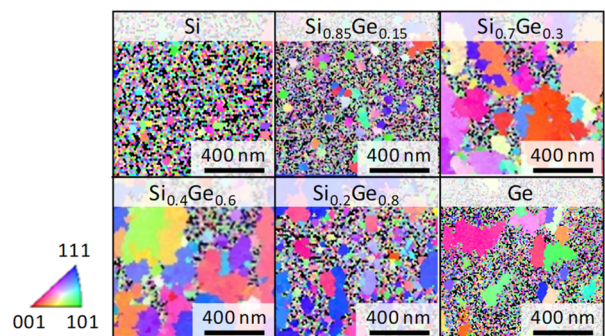


**FIG. 3.** IPF images of  $\text{Si}_{1-x}\text{Ge}_x$  ( $x=0, 0.15, 0.3, 0.6, 0.8$ , and 1) on glass obtained by EBSD analyses. The colors indicate the crystal orientation according to the color key.

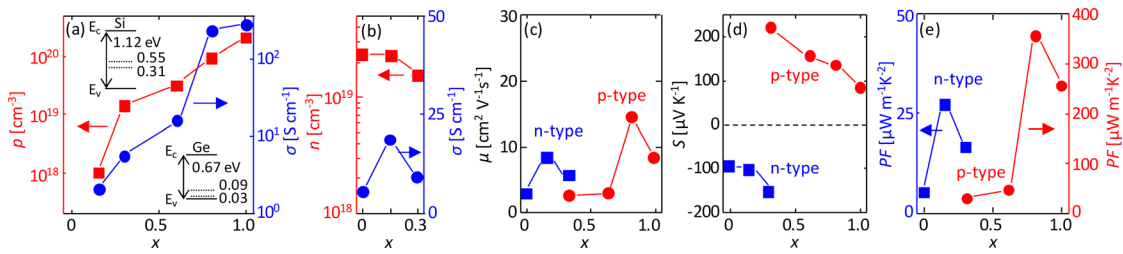


**FIG. 4.** Electrical and thermoelectric properties at RT as a function of  $x$  for  $\text{Si}_{1-x}\text{Ge}_x$  ( $x = 0, 0.15, 0.3, 0.6, 0.8,$  and  $1$ ) on glass formed by LE using Zn or As-doped Zn. (a) Hole concentration  $p$  and electrical conductivity  $\sigma$  for  $x = 0.15-1$ , where the impurity levels of Zn in Si and Ge are shown on the graph. (b) Electron concentration  $n$  and  $\sigma$  for  $x = 0-0.3$ . (c) Carrier mobility  $\mu$ , (d) Seebeck coefficient  $S$ , and (e) power factor  $PF$  for n-type  $\text{Si}_{1-x}\text{Ge}_x$  ( $x = 0-0.3$ ) and p-type  $\text{Si}_{1-x}\text{Ge}_x$  ( $x = 0.3-1$ ).

slope with respect to  $T$  as  $x$  decreases. This behavior suggests that the acceptor levels due to Zn in SiGe become deeper as  $x$  decreases. The Ge-rich  $\text{Si}_{1-x}\text{Ge}_x$  ( $x \geq 0.8$ ) exhibits  $\sigma$  higher than  $200 \text{ S/cm}$ , which is useful as a p-type thermoelectric thin film. In contrast, Si-rich  $\text{Si}_{1-x}\text{Ge}_x$  ( $x \leq 0.3$ ) has a low  $\sigma$  due to low  $p$ . Therefore, n-type conduction control could be affected by adding n-type impurities to the Si-rich  $\text{Si}_{1-x}\text{Ge}_x$  ( $x \leq 0.3$ ). The LE of a- $\text{Si}_{1-x}\text{Ge}_x$  ( $x \leq 0.3$ ) using As-doped Zn was achieved when the initial As concentration of Zn was 10% or less. Therefore, the initial As concentration in Zn was fixed at  $\sim 10\%$  for all the samples, which resulted in the electron concentration  $n$  exceeding  $10^{19} \text{ cm}^{-3}$ , as shown in Fig. 4(b). Since  $n$  decreased with increasing  $x$ , this possibly reflects the solubility limit of As in SiGe.<sup>40</sup> Although  $\sigma$  is one order lower than that of p-type Ge-rich SiGe, the synthesis temperature ( $350^\circ\text{C}$ ) is the lowest observed for n-type SiGe layers. Figure 4(c) shows that the carrier mobility  $\mu$  does not have a clear tendency for  $x$ . This is because  $\mu$  is affected by various factors including the carrier effective mass, grain size, grain boundary barrier height, and carrier concentration.<sup>41</sup> The  $S$  value corresponding to the appropriate conduction type was obtained for each of the p-type SiGe ( $x \geq 0.3$ ) and the n-type SiGe ( $x \leq 0.3$ ). Figure 4(d) shows the strong dependence of  $S$  on  $x$ :  $|S|$  decreases with increasing  $x$  for p-type SiGe;  $|S|$  increases with increasing  $x$  for n-type SiGe. Generally,  $S$  is affected by both the carrier concentration and the  $\mu$  value.<sup>2,3</sup> Considering the results in Figs. 4(a)–4(c), the current dependence of  $S$  on  $x$  mainly reflects the carrier concentration. Figure 4(e) shows that the  $PF$  reaches approximately  $30 \mu\text{W/mK}^2$  for n-type SiGe at  $x = 0.15$  and  $360 \mu\text{W/mK}^2$  for p-type SiGe at  $x = 0.8$ . The difference in the  $PF$  between the p-type and the n-type is attributed mainly to the difference in the carrier concentration directly linked to  $\sigma$ . A more active n-type dopant, such as phosphorus, is expected to improve the  $PF$  of the n-type SiGe layer.

Since both p-type  $\text{Si}_{0.2}\text{Ge}_{0.8}$  and n-type  $\text{Si}_{0.85}\text{Ge}_{0.15}$  can be synthesized at a low temperature ( $350^\circ\text{C}$ ), we fabricated them on a flexible plastic sheet. The substrate was  $125\text{-}\mu\text{m}$ -thick polyimide (Du Pont-Toray Co., Ltd.), pre-covered with a sputtered  $100 \text{ nm}$  thick  $\text{SiO}_2$  layer. Figure 5(a) shows the flexibility of the sample even after the LE process. Figure 5(b) shows that the dependence of  $\sigma$  on  $T$  is opposite for the p-type and the n-type, i.e.,  $\sigma$  decreases with increasing  $T$  for p-type SiGe, while it increases with increasing  $T$  for n-type SiGe. For p-type SiGe, this is a typical trend of the degenerated semiconductor exhibiting metallic behavior, which is attributed to the high  $p$  value.<sup>2,3</sup> Conversely, the trend of n-type SiGe differs from that of the single-crystal SiGe, suggesting that  $\sigma$  is dominantly limited by grain boundary carrier scattering.<sup>41</sup> The samples with a plastic substrate exhibit

lower  $\sigma$  compared to the samples with a glass substrate. Considering the fact that the plastic samples had smaller grains (almost below the EBSD resolution) than the glass samples, the difference in  $\sigma$  between the substrates reflects grain boundary scattering. This behavior was also observed in the SiGe–Al system and explained from the perspective of the strains during LE.<sup>22,34</sup> The plastic substrate bends slightly during annealing and strains the upper layers, which facilitates SiGe nucleation and reduces the size of the resulting SiGe grains. Figure 5(c) shows that  $|S|$  increases with increasing  $T$  for both p- and n-type SiGe on the glass and plastic substrates, which is typical for SiGe with carrier concentrations on the order of  $10^{19}-10^{20} \text{ cm}^{-3}$ .<sup>2</sup>  $S$  is almost the same for the samples on the glass and plastic substrates. Figure 5(d) shows that the  $PF$  increases with increasing  $T$  for all samples, reflecting the  $T$  dependence of  $\sigma$  and  $S$ . The  $PF$  at RT is estimated to be  $280 \mu\text{W/mK}^2$  for the p-type and  $15 \mu\text{W/mK}^2$  for the n-type for the plastic samples. Although there is significant scope for improving the performance, especially for n-type SiGe, these  $PF$  values are the best values recorded for p- and n-type SiGe on a plastic substrate.

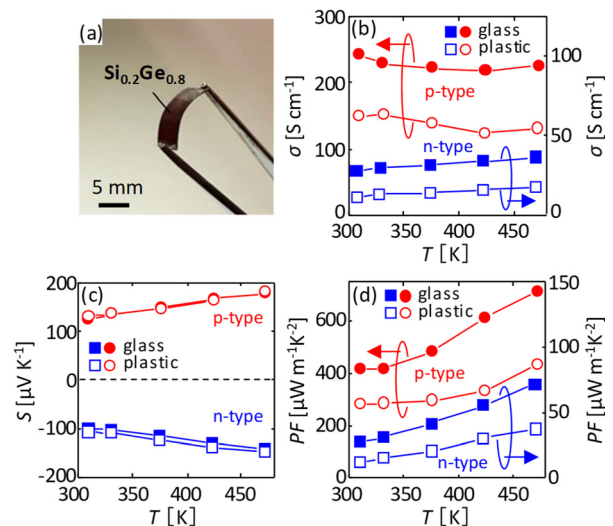


**FIG. 5.** Thermoelectric properties of p-type  $\text{Si}_{0.2}\text{Ge}_{0.8}$  and n-type  $\text{Si}_{0.85}\text{Ge}_{0.15}$  formed on glass (solid symbol) and a plastic substrate (open symbol) with respect to the measurement temperature  $T$ . (a) Photograph of p-type  $\text{Si}_{0.2}\text{Ge}_{0.8}$  on the plastic substrate after Zn removal. (b) Electrical conductivity  $\sigma$ . (c) Seebeck coefficient  $S$ . (d) Power factor  $PF$ .

In conclusion, Zn-induced LE enabled us to fabricate both p- and n-type nanocrystalline  $\text{Si}_{1-x}\text{Ge}_x$  layers at low temperatures (120–350 °C) in the whole composition range. Pure Zn formed p-type SiGe due to the shallow acceptor level of Zn in Ge and allowed for high  $p$  over  $10^{20} \text{ cm}^{-3}$  for  $x \geq 0.8$ . For  $x \leq 0.3$ , LE using As-doped Zn enabled the self-organized doping of As to SiGe and achieved n-type SiGe with  $n$  over  $10^{19} \text{ cm}^{-3}$  even at the low fabrication temperature. The p-type  $\text{Si}_{0.2}\text{Ge}_{0.8}$  and n-type  $\text{Si}_{0.85}\text{Ge}_{0.15}$  layers fabricated on a plastic substrate exhibited  $PF$  values of  $280 \mu\text{W/mK}^2$  and  $15 \mu\text{W/mK}^2$ , respectively. The dynamic Fermi-level control in SiGe via a low-temperature process could be exploited by various flexible devices including TEGs, with a high reliability.

This work was financially supported by the JST PRESTO (No. JPMJPR17R7) and the Thermal & Electric Energy Technology Foundation. The authors are grateful to Professor T. Sakurai (University of Tsukuba) with the Hall effect measurements. Some experiments were conducted at the International Center for Young Scientists in NIMS and the Nanotechnology Platform at the University of Tsukuba.

The data that support the findings of this study are available from the corresponding author upon reasonable request.

## REFERENCES

- <sup>1</sup>K. Petsagkourakis, K. Tybrandt, X. Crispin, I. Ohkubo, N. Satoh, and T. Mori, *Sci. Technol. Adv. Mater.* **19**, 836 (2018).
- <sup>2</sup>J. P. Dismukes, L. Ekstrom, E. F. Steigmeier, I. Kudman, and D. S. Beers, *J. Appl. Phys.* **35**, 2899 (1964).
- <sup>3</sup>C. B. Vining, *J. Appl. Phys.* **69**, 331 (1991).
- <sup>4</sup>K. Tajima, W. Shin, M. Nishibori, N. Murayama, T. Itoh, N. Izu, and I. Matsubara, *Key Eng. Mater.* **320**, 99 (2006).
- <sup>5</sup>J. A. Perez-Taborda, M. Muñoz Rojo, J. Maiz, N. Neophytou, and M. Martin-Gonzalez, *Sci. Rep.* **6**, 32778 (2016).
- <sup>6</sup>M. Takashiri, T. Borca-Tasciuc, A. Jacquot, K. Miyazaki, and G. Chen, *J. Appl. Phys.* **100**, 054315 (2006).
- <sup>7</sup>R. Cheaito, J. C. Duda, T. E. Beechem, K. Hattar, J. F. Ihlefeld, D. L. Medlin, M. A. Rodriguez, M. J. Campion, E. S. Piekos, and P. E. Hopkins, *Phys. Rev. Lett.* **109**, 195901 (2012).
- <sup>8</sup>J. Lu, R. Guo, and B. Huang, *Appl. Phys. Lett.* **108**, 141903 (2016).
- <sup>9</sup>A. Nozariasbmarz, A. Tahmasbi Rad, Z. Zamanipour, J. S. Krasinski, L. Tayebi, and D. Vashaee, *Scr. Mater.* **69**, 549 (2013).
- <sup>10</sup>H. Takiguchi, M. Aono, and Y. Okamoto, *Jpn. J. Appl. Phys., Part 1* **50**, 041301 (2011).
- <sup>11</sup>M. Lindorf, H. Rohrmann, G. Span, S. Raoux, J. Jordan-Sweet, and M. Albrecht, *J. Appl. Phys.* **120**, 205304 (2016).
- <sup>12</sup>M. Koike, Y. Kamata, T. Ino, D. Hagishima, K. Tatsumura, M. Koyama, and A. Nishiyama, *J. Appl. Phys.* **104**, 023523 (2008).
- <sup>13</sup>H. Haesslein, R. Sielemann, and C. Zistl, *Phys. Rev. Lett.* **80**, 2626 (1998).
- <sup>14</sup>D. Takahara, R. Yoshimine, T. Suemasu, and K. Toko, *J. Alloys Compd.* **766**, 417 (2018).
- <sup>15</sup>O. Nast, T. Puzzer, L. M. Koschier, A. B. Sproul, and S. R. Wenham, *Appl. Phys. Lett.* **73**, 3214 (1998).
- <sup>16</sup>A. Sarikov, J. Schneider, J. Berghold, M. Muske, I. Sieber, S. Gall, and W. Fuhs, *J. Appl. Phys.* **107**, 114318 (2010).
- <sup>17</sup>Z. Wang, L. Gu, L. P. H. Jeurgens, F. Phillipp, and E. J. Mittemeijer, *Nano Lett.* **12**, 6126 (2012).
- <sup>18</sup>K. Toko, R. Numata, N. Saitoh, N. Yoshizawa, N. Usami, and T. Suemasu, *J. Appl. Phys.* **115**, 094301 (2014).
- <sup>19</sup>S. Hu, A. F. Marshall, and P. C. McIntyre, *Appl. Phys. Lett.* **97**, 082104 (2010).
- <sup>20</sup>K. Toko, R. Numata, N. Oya, N. Fukata, N. Usami, and T. Suemasu, *Appl. Phys. Lett.* **104**, 022106 (2014).
- <sup>21</sup>J.-H. Park, K. Kasahara, K. Hamaya, M. Miyao, and T. Sadoh, *Appl. Phys. Lett.* **104**, 252110 (2014).
- <sup>22</sup>N. Oya, K. Toko, N. Saitoh, N. Yoshizawa, and T. Suemasu, *Thin Solid Films* **583**, 221 (2015).
- <sup>23</sup>R. Yoshimine, K. Toko, N. Saitoh, N. Yoshizawa, and T. Suemasu, *J. Appl. Phys.* **122**, 215305 (2017).
- <sup>24</sup>H. Higashi, K. Kudo, K. Yamamoto, S. Yamada, T. Kanashima, I. Tsunoda, H. Nakashima, and K. Hamaya, *J. Appl. Phys.* **123**, 215704 (2018).
- <sup>25</sup>H. Murata, N. Saitoh, N. Yoshizawa, T. Suemasu, and K. Toko, *Appl. Phys. Lett.* **111**, 243104 (2017).
- <sup>26</sup>Y. Nakajima, H. Murata, N. Saitoh, N. Yoshizawa, T. Suemasu, and K. Toko, *ACS Appl. Mater. Interfaces* **10**, 41664 (2018).
- <sup>27</sup>M. Gjukic, M. Buschbeck, R. Lechner, and M. Stutzmann, *Appl. Phys. Lett.* **85**, 2134 (2004).
- <sup>28</sup>T. Iwasa, T. Kaneko, I. Nakamura, and M. Isomura, *Phys. Status Solidi* **207**, 617 (2010).
- <sup>29</sup>M. Kurosawa, N. Kawabata, T. Sadoh, and M. Miyao, *ECS J. Solid State Sci. Technol.* **1**, P144 (2012).
- <sup>30</sup>T. Zhang, F. Ma, and W. Zhang, *Appl. Phys. Lett.* **100**, 071908 (2012).
- <sup>31</sup>C. A. Niedermeier, Z. Wang, and E. J. Mittemeijer, *Acta Mater.* **72**, 211 (2014).
- <sup>32</sup>M. Nakata, K. Toko, N. Saitoh, N. Yoshizawa, and T. Suemasu, *Scr. Mater.* **122**, 86 (2016).
- <sup>33</sup>K. Toko, K. Kusano, M. Nakata, and T. Suemasu, *J. Appl. Phys.* **122**, 155305 (2017).
- <sup>34</sup>K. Kusano, A. Yamamoto, M. Nakata, T. Suemasu, and K. Toko, *ACS Appl. Energy Mater.* **1**, 5280 (2018).
- <sup>35</sup>M. Tsuji, T. Imajo, N. Saitoh, N. Yoshizawa, T. Suemasu, and K. Toko, *J. Phys. D: Appl. Phys.* **53**, 075105 (2020).
- <sup>36</sup>K. Kusano, M. Tsuji, T. Suemasu, and K. Toko, *Appl. Phys. Express* **12**, 055501 (2019).
- <sup>37</sup>S. M. Sze and J. C. Irvin, *Solid State Electron.* **11**, 599 (1968).
- <sup>38</sup>P. M. Mooney, F. H. Dacol, J. C. Tsang, and J. O. Chu, *Appl. Phys. Lett.* **62**, 2069 (1993).
- <sup>39</sup>Y. Nakamura, M. Isogawa, T. Ueda, S. Yamasaka, H. Matsui, J. Kikkawa, S. Ikeuchi, T. Oyake, T. Hori, J. Shiomi, and A. Sakai, *Nano Energy* **12**, 845 (2015).
- <sup>40</sup>F. A. Trumbore, *Bell Syst. Tech. J.* **39**, 205 (1960).
- <sup>41</sup>J. W. Y. Seto, *J. Appl. Phys.* **46**, 5247 (1975).